

OPEN

# Multiparametric Magnetic Resonance Imaging of Prostate Cancer Bone Disease

## Correlation With Bone Biopsy Histological and Molecular Features

Raquel Perez-Lopez, MD, PhD,\*† Daniel Nava Rodrigues, MD,† Ines Figueiredo, BSc,†  
Joaquin Mateo, MD, MSc,\*† David J. Collins, BMIP,\*† Dow-Mu Koh, MD, FRCR, MRCP,\*†  
Johann S. de Bono, MB, ChB, PhD,\*† and Nina Tunariu, MD, FRCR, MRCP\*†

**Objectives:** The aim of this study was to correlate magnetic resonance imaging (MRI) of castration-resistant prostate cancer (CRPC) bone metastases with histological and molecular features of bone metastases.

**Materials and Methods:** Forty-three bone marrow biopsies from 33 metastatic CRPC (mCRPC) patients with multiparametric MRI and documented bone metastases were evaluated. A second cohort included 10 CRPC patients with no bone metastases. Associations of apparent diffusion coefficient (ADC), normalized b900 diffusion-weighted imaging (nDWI) signal, and signal-weighted fat fraction (swFF) with bone marrow biopsy histological parameters were evaluated using Mann-Whitney *U* test and Spearman correlations. Univariate and multivariate logistic regression models were analyzed.

**Results:** Median ADC and nDWI signal was significantly higher, and median swFF was significantly lower, in bone metastases than nonmetastatic bone ( $P < 0.001$ ). In the metastatic cohort, 31 (72.1%) of 43 biopsies had detectable cancer cells. Median ADC and swFF were significantly lower and median nDWI signal was significantly higher in biopsies with tumor cells versus nondetectable tumor cells ( $898 \times 10^{-6} \text{ mm}^2/\text{s}$  vs  $1617 \times 10^{-6} \text{ mm}^2/\text{s}$ ; 11.5% vs 62%; 5.3 vs 2.3, respectively;  $P < 0.001$ ). Tumor cellularity inversely correlated with ADC and swFF, and positively correlated with nDWI signal ( $P < 0.001$ ). In serial biopsies, taken before and after treatment, changes in multiparametric MRI parameters paralleled histological changes.

**Conclusions:** Multiparametric MRI provides valuable information about mCRPC bone metastases. These data further clinically qualify DWI as a response biomarker in mCRPC.

**Key Words:** prostate cancer, bone metastases, multiparametric MRI, diffusion-weighted imaging, biopsies

(*Invest Radiol* 2018;53: 96–102)

**T**herapeutic options for patients with metastatic castration-resistant prostate cancer (mCRPC) have increased over the last decade

with the approval of several agents improving overall survival.<sup>1–4</sup> Yet, as progression on these treatments inevitably ensues, mCRPC remains a fatal condition. For optimal development of more precise therapeutic strategies, there is a need for the clinical qualification of predictive biomarkers, which requires acquisition of tumor material, and better response biomarkers to guide therapeutic decisions.

Bone metastases are the most common (>80%) metastatic site in advanced mCRPC; in more than 40% of the patients, these represent the sole site of metastatic spread.<sup>5</sup> Although metastatic bone marrow biopsies have been successfully implemented in prior studies,<sup>6</sup> acquiring these samples remains difficult as bone marrow biopsies can yield specimens with poor tumor content due to increased sclerosis or response to previous therapies. Imaging that could increase the likelihood of obtaining high-quality tumor samples remains a highly desirable goal.<sup>7</sup> Furthermore, standardized imaging response criteria for bone metastases remain a major unmet medical need.<sup>8,9</sup>

Multiparametric (MP) magnetic resonance imaging (MRI) including T1-weighted sequences, diffusion-weighted imaging (DWI), and Dixon quantitative chemical shift imaging-derived fat fraction (FF) allows the study of anatomical and functional features of bone marrow. Diffusion-weighted imaging studies the random movement of water molecules within a tissue and has high sensitivity and specificity for the detection of bone metastases.<sup>10</sup> Multiple studies have previously shown a strong correlation between apparent diffusion coefficient (ADC), the quantitative parameter derived from DWI, and tissue cellularity in soft tissue tumors.<sup>11–17</sup> In addition, several studies have shown significant ADC differences between normal bone marrow and malignancies in the bone.<sup>18–20</sup> However, only limited data are available correlating DWI parameters with cellularity and other histological features in bone metastases.<sup>21,22</sup> Translational studies correlating functional imaging and the underlying histology are critical for clinical qualification of MP-MRI as a prognostic and response biomarker in prostate cancer bone metastases.

Normal bone marrow contains both fat and water (yellow marrow approximately 80% fat; red marrow approximately 40% fat).<sup>23</sup> Malignant cells displace the bone marrow fat cells causing a reduction in fat content; conversely, successful therapies are associated with return of normal bone marrow fat.<sup>24</sup> Dixon quantitative chemical shift imaging uses the difference in resonance frequency between water and fat to estimate FF of a tissue.<sup>23</sup>

We hypothesized that MP-MRI provided accurate in vivo information about bone metastases characteristics. We correlated MRI quantitative parameters of mCRPC bone metastases within the biopsy tract, including ADC, normalized b900 DWI (nDWI) signal intensity, and signal-weighted fat fraction (swFF), with histological and molecular bone biopsy features including tumor cell burden, immature osteoid burden, fibrosis, proportion of fat, expression for the phosphatase and tensin homolog (*PTEN*, a tumor suppressor gene frequently deleted or mutated in prostate cancer resulting in lack of protein expression), and Ki67 proliferation index. We also assessed the MP-MRI features of normal bone marrow in a subgroup of patients with prostate cancer and no evidence of bone metastases on multimodality imaging.

Received for publication June 12, 2017; and accepted for publication, after revision, July 29, 2017.

From the \*The Institute of Cancer Research; and †The Royal Marsden NHS Foundation Trust, London, United Kingdom.

Funding information: Prostate Cancer UK (PG14-016-TR2), Prostate Cancer Foundation (20131017), Stand Up To Cancer (SU2C-AACR-DT0712), Movember Foundation (Movember-Prostate Cancer UK Centre Grant CEO13-2-002), and Cancer Research UK (C347/A18077 and CRUK C1060/A16464).

R.P.L. and D.N.R. are joint first authors.

Supplemental digital contents are available for this article. Direct URL citations appear in the printed text and are provided in the HTML and PDF versions of this article on the journal's Web site ([www.investigativeradiology.com](http://www.investigativeradiology.com)).

Correspondence to: Nina Tunariu, MD, FRCR, MRCP, Radiology Consultant at The Royal Marsden NHS Foundation Trust, Downs Road, SM2 5PT, London, United Kingdom. E-mail: [Nina.Tunariu@icr.ac.uk](mailto:Nina.Tunariu@icr.ac.uk)

Copyright © 2017 The Author(s). Published by Wolters Kluwer Health, Inc. This is an open-access article distributed under the terms of the Creative Commons Attribution-Non Commercial-No Derivatives License 4.0 (CCBY-NC-ND), where it is permissible to download and share the work provided it is properly cited. The work cannot be changed in any way or used commercially without permission from the journal.

ISSN: 0020-9996/18/5302-0096

DOI: 10.1097/RLI.0000000000000415

## MATERIALS AND METHODS

This was a retrospective study conducted under Royal Marsden Research Ethics Committee approval. Written informed consent was obtained from all patients.

### Patient Population

We reviewed all consecutive posterior iliac crest bone marrow biopsies and MP-MRI in mCRPC patients at The Royal Marsden Hospital (United Kingdom) performed between May 2012 and March 2016 as part of a prospective molecular characterization study.<sup>6</sup> Study inclusion criteria were (a) bone metastases in the posterior iliac crest, corresponding to the area of the routine bone marrow biopsy, based on computed tomography (CT), bone scan (BS), and MRI; (b) MP-MRI within 12 weeks before the bone biopsy; and (c) presence of a visible bone biopsy tract in the posterior iliac crest on a subsequent CT. Cases were excluded if (a) bone biopsy did not include bone tissue or (b) MP-MRI study had suboptimal DWI due to artifacts or was incomplete.

A second control cohort included 10 consecutive patients who underwent MP-MRI but had no detectable bone metastases on a CT and BS performed with 12 weeks of the MP-MRI and either on the MP-MRI; no bone biopsies were obtained in this cohort for ethical reasons. To be included in the control cohort, cases had to (1) have a prior diagnosis of prostate cancer, (2) be under castration treatment, and (3) have both a CT and a BS performed within 12 weeks of the MP-MRI.

### Clinical Data Collection

Data from patient records were collected into an anonymized database; these included age, prior treatments, and laboratory parameters at the time of the MRI. The presence of bone metastases was assessed based on CT and BS performed at any time point before the bone biopsy

and MP-MRI performed within 12 weeks before the bone biopsy, in all cases.

### Histological and Molecular Parameters

Bone biopsies were decalcified in 14% EDTA and processed as previously described.<sup>7</sup> Sections were cut at 2  $\mu$ m onto glass slides and stained with hematoxylin and eosin. A pathologist (D.N.R.) blinded to clinical and radiological data reviewed the biopsies. Tumor cellularity was semiquantitatively scored into 4 tiers: 0 (no tumor cells), +1 ( $\leq$ 50 tumor cells), +2 (50–250 tumor cells), and +3 ( $\geq$ 250 tumor cells) by section. Trabecular volume was semiquantitatively calculated as described by Teman et al.<sup>25</sup> Gross fibrosis and immature osteoid (woven bone) content were semiquantitatively scored as follows: 0 (absent), +1 (present in  $<$ 1/3 of biopsy), +2 ( $\geq$ 1/3 to  $<$ 2/3 of biopsy), and +3 ( $\geq$ 2/3 of biopsy). Fat content was defined as the area occupied by fat/total biopsy area ( $\times$ 100). *PTEN* and *Ki67* were assessed by immunohistochemistry as previously described.<sup>26</sup> *PTEN* loss was defined as H-score of 10 or lower.

### MP-MRI Parameters

Multiparametric-MRI was performed on a 1.5 T MRI scanner (Magnetom Avanto or Aera Siemens Healthcare, Erlangen, Germany), using surface and body coils on patients positioned supine (Supplemental Digital Content 1, Supplementary Table 1, <http://links.lww.com/RLI/A346>). The DWI was performed in axial plane using *b*-values of 50 and 900 s/mm<sup>2</sup>. The swFF maps were calculated using an in-house Osirix plug-in [ $FF = 100\% \times S_{fat}/(S_{fat} + S_{water})$ , where *S* indicates signal at every voxel location].

### MRI and CT Analysis

Images were processed and analyzed with open-access imaging assistant software (Osirix v5.6) by a single radiologist (R.P.L.), blinded

**TABLE 1.** Population Characteristics of Patients With Bone Metastases and Biopsies (n = 43) and Those With No Bone Metastases Who Did Not Have Biopsies (n = 10)

Previous Treatments	Cohort With Bone Metastases and Biopsies (n = 43), n (%)	Cohort With No Bone Metastases and No Biopsies (n = 10), n (%)
Prostate radiotherapy	14 (32.6%)	5 (50%)
Pelvic bone radiotherapy	19 (44.2%)	0 (0%)
Abiraterone	36 (83.3%)	0 (0%)
Enzalutamide	15 (34.9%)	0 (0%)
Docetaxel	32 (74.4%)	0 (0%)
Cabazitaxel	18 (41.9%)	0 (0%)
Cabozantinib	3 (7.0%)	0 (0%)
Rad 223	5 (11.6%)	0 (0%)
Bisphosphonates	10 (23.3%)	0 (0%)
Clinical Characteristics	Median (IQR)	Median (IQR)
PSA, ng/mL	345 (126–806)	23 (6–26)
CTC, cells per 7.5 mL of blood	18 (6–121)	—
Hemoglobin, g/dL	112 (106–125)	140 (132–155)
Alkaline phosphatase, IU/L	164 (105–423)	56 (52–65)
Lactate dehydrogenase, IU/L	189 (165–239)	198 (162–200)
Bone Scan Index (%)	Median (IQR)	
Total biopsy cohort (n = 35)	5.6 (2.6–10.2)	—
Biopsy positive for tumor cells (n = 25)	5.6 (3.6–9.2)	—
Biopsy negative for tumor cells (n = 10)	5.5 (1.0–10.1)	—

CTC indicates circulating tumor cells; IQR, interquartile range; PSA, prostate specific antigen.

to pathology and molecular data. The biopsy tract was identified on a postbiopsy axial CT; a 2-dimensional region of interest (ROI) delineating the biopsy tract was manually drawn. In the population with no bone metastases, 2 bilateral ROIs delineating the posterior-superior iliac crests at 1 level, representative for where standard bone marrow biopsies are usually performed, were manually drawn. The axial CT and DWI sequences (b900, ADC, and FF maps) taken prebiopsy were coregistered using the Osirix Insight Segmentation and Registration Toolkit<sup>27,28</sup>; the ROIs were then transferred to the b900 images, ADC, and swFF maps. To perform DWI signal normalization, ROI muscle were delineated on b900 images within the gluteus maximus muscle at the same side and level as the iliac crest bone marrow biopsy; nDWI was defined as the ratio of biopsy tract b900 signal intensity to muscle ROI b900 signal intensity. The following data were collated for each ROI on MRI: nDWI signal intensity, ADC, and swFF.

If a CT was performed within 12 weeks of the bone biopsy, coregistration of the CT prebiopsy and postbiopsy was performed; CT density (Hounsfield units [HU]) of the ROI corresponding to the biopsy tract in the prebiopsy CT scan images was recorded.

### BS Analysis

If a whole-body BS had been performed within 12 weeks before the bone biopsy, bone scan index (BSI) was calculated using an automated BSI scoring software (Exini Diagnostics, Lund, Sweden).<sup>29</sup>

### Statistical Analysis

Descriptive statistics were used to summarize the baseline clinical, histological, and molecular characteristics and imaging features. Differences in MP-MRI and CT parameters between regions positive and negative for tumor cells on bone biopsy were assessed using Mann-Whitney *U* tests. Univariate analyses were performed using logistic regression models. Variables with a statistically significant association to bone biopsy positivity for tumor cells ( $P < 0.05$ ) were included in a multivariate logistic regression model. Correlations between MP-MRI, histological, and molecular parameters were assessed using Spearman correlation (*r*). The performance of the imaging biomarkers was evaluated by receiver operating characteristic curve analysis and linear discriminant analysis. Statistical analyses were performed with Stata version 13 (StataCorp) and SPSS version 20 (IBM).

## RESULTS

### Patient and Bone Biopsy Characteristics

The flowchart of the study selection process is shown in Supplemental Digital Content 2, Supplementary Figure 1, <http://links.lww.com/RLI/A347>. In the cohort of patients with bone metastases, 43 bone biopsies from 33 patients (all male; median age, 72 years; range, 48–84 years) were evaluable. Thirty-one (72.1%) of these 43 biopsies were positive for tumor cells with 12 (27.9%) of 43 having no tumor cells. In the cohort of patients with no detectable bone metastases, 10 CRPC patients were included (all male; median age, 69 years; range, 53–75 years). The population characteristics are summarized in Table 1. The histological and molecular characteristics of the bone biopsies are summarized in Table 2.

### MP-MRI of Bone With or Without Prostate Cancer Bone Metastases

The median ADC of bone metastases was significantly higher than in nonmetastatic iliac crests:  $993 \times 10^{-6} \text{ mm}^2/\text{s}$  (interquartile range [IQR],  $872.5\text{--}1093.5 \times 10^{-6} \text{ mm}^2/\text{s}$ ) and  $601.8 \times 10^{-6} \text{ mm}^2/\text{s}$  (IQR,  $545\text{--}667 \times 10^{-6} \text{ mm}^2/\text{s}$ ), respectively ( $P < 0.001$ ). The median nDWI signal was 4 (IQR, 2.6–6.7) in the bone metastases cohort and 1.6 (IQR, 1.4–2.7) in the cohort without bone metastases ( $P < 0.001$ ). The median swFF in bone metastases was 16% (IQR, 9%–45%),

**TABLE 2.** Histological and Molecular Characteristics of the Bone Biopsies (n = 43)

Histological Characteristics	n (%)
Osteoid	
0	0 (0%)
1	9 (20.9%)
2	16 (37.2%)
3	18 (41.9%)
Fibrosis	
0	4 (9.3%)
1	11 (25.6%)
2	8 (18.6%)
3	20 (46.5%)
Cellularity	
0	12 (27.9%)
1	6 (13.9%)
2	9 (20.9%)
3	16 (37.2%)
Fat area	Median (IQR)
%	25% (5%–50%)
<b>Molecular Characteristics</b>	
<i>PTEN</i> expression (n = 22; unknown n = 21)	
<i>PTEN</i> loss	8 (36.3%)
<i>PTEN</i> present	14 (66.6%)
Ki67 (n = 25; unknown n = 18)	Median (IQR)
%	25% (10%–50%)

significantly lower than in nonmetastatic bone, which was 63% (IQR, 60%–76%;  $P < 0.001$ ).

### Bone Metastases: MRI and Histological Parameters

The median ADC in the region of bone biopsies containing tumor was  $898 \times 10^{-6} \text{ mm}^2/\text{s}$  (IQR,  $816\text{--}1019 \times 10^{-6} \text{ mm}^2/\text{s}$ ), compared with  $1617 \times 10^{-6} \text{ mm}^2/\text{s}$  (IQR,  $1067\text{--}1787.5 \times 10^{-6} \text{ mm}^2/\text{s}$ ) in bone with no visible tumor cells in the bone biopsy ( $P < 0.001$ ). The median nDWI signal was significantly higher in bone biopsies containing tumor cells (5.3 [IQR, 3.1–7.8]) compared with those with no detectable tumor cells (2.3 [IQR, 2–3.3];  $P < 0.001$ ). Moreover, the median swFF in positive bone biopsies was 11.45% (IQR, 8.5%–17%) compared with 62% (IQR, 45%–82.9%) in bone biopsies not containing tumor ( $P < 0.001$ ) (Fig. 1; Supplemental Digital Content 3, Supplementary Figure 2, <http://links.lww.com/RLI/A348>). Receiver operating characteristic area under the curve values were 0.86 (95% confidence interval [CI], 0.64–1.00) for median ADC, 0.87 (95% CI, 0.68–0.98) for median nDWI signal, and 0.90 (95% CI, 0.74–1.00) for median swFF (Supplemental Digital Content 4, Supplementary Figure 3, <http://links.lww.com/RLI/A349>).

We then evaluated whether the combination of these parameters could improve their performance, using Linear Discriminant Analysis. Because of the high correlation between median nDWI and median ADC ( $P < 0.001$ ), only median ADC and median swFF were considered in the model. The function combining median ADC and median swFF was able to significantly discriminate biopsies with tumor from biopsies without tumor and nonmetastatic bone (Wilks  $\lambda = 0.31$ ;  $P < 0.001$ ). The function combining median ADC and median swFF had a sensitivity of 80% and a specificity of 96% for the detection of a positive bone marrow biopsy; 91.4% of the cases were correctly

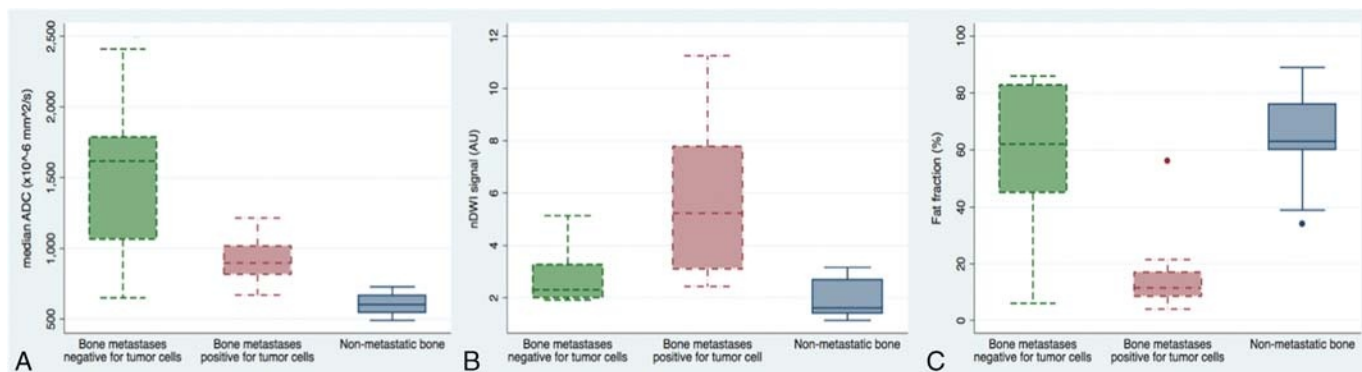


**FIGURE 1.** Box plots of the distribution of (A) median ADC, (B) median nDWI signal intensity, and (C) median swFF of the bone marrow in patients with bone metastases and bone biopsy negative for tumor cells (green), bone metastases and bone biopsy positive for tumor cells (red), and no bone metastases (blue).

classified by the function (Supplemental Digital Content 5, Supplementary Table 2, <http://links.lww.com/RLI/A350>).

There was an inverse correlation between histological cellularity burden as an ordinal variable and ADC ( $P < 0.001$ ) and swFF ( $P < 0.001$ ), as well as a positive correlation with nDWI signal intensity ( $P < 0.001$ ). We also observed a positive correlation between the median swFF on MP-MRI and percentage of histological fat content in the bone biopsies ( $P < 0.001$ ) (Table 3).

Immature osteoid and fibrosis in the bone biopsies were associated with positive biopsy results; in multivariate analysis, median ADC remained independently associated with biopsy positivity for tumor cells ( $P = 0.050$ ) (Table 4).

In our series, median ADC of bone metastases did not correlate with Ki67 proliferation index ( $r = 0.28, P = 0.180$ ) or loss of *PTEN* expression ( $r = -0.34, P = 0.118$ ).

### Evaluating Bone Metastases by CT and BS

For 39 (90.7%) of 43 biopsies in the bone metastases cohort, a CT scan performed within 12 weeks before the biopsy was also available. All the 10 patients in the cohort without bone metastases also had a CT scan performed within 12 weeks of the MP-MRI.

Computed tomography density was significantly higher in the presence of metastatic disease than in the bone with no metastases (median, 252 HU; IQR, 191–337.50 HU vs 67 HU; IQR 35–85 HU;  $P < 0.001$ ).

In the metastatic cohort, 29 (74.4%) of the 39 patients with a CT scan performed within 12 weeks of the bone biopsy had positive biopsies containing tumor cells. The median HU on CT was not significantly different for bone metastases with positive biopsy compared with those with negative biopsy without tumor cells present (median, 278 HU

**TABLE 3.** Correlation Between MP-MRI and Histological Parameters Generated From Bone Biopsy Analyses (Spearman *r* Correlation Coefficient)

	<i>r</i>	<i>P</i>
Correlation with bone metastasis cellularity		
Median ADC	-0.57	<0.001
Median nDWI signal intensity	0.59	<0.001
Signal-weighted fat fraction	-0.59	<0.001
Correlation with bone metastasis fat content		
Signal-weighted fat fraction	0.60	<0.001

ADC indicates apparent diffusion coefficient; MP, multiparametric; MRI, magnetic resonance imaging; nDWI, normalized b900 diffusion-weighted imaging.

[IQR 139–348 HU] vs 241 HU [IQR 192–327 HU];  $P = 0.966$ ) (Supplemental Digital Content 6, Supplementary Figure 4, <http://links.lww.com/RLI/A351>).

Furthermore, in 35 (81.4%) of 43 biopsies, a BS was performed within 12 weeks (median, 2.7 weeks; IQR, 0.5–7.3 weeks) of the biopsy with DICOM images allowing BSI calculation. Twenty-five (71.4%) of these 35 biopsies were positive for tumor cells. The BSI was not significantly different in the group of patients with a positive biopsy compared with those with negative biopsy (median, 5.6 [IQR, 3.6–9.2] vs 5.5 [IQR, 1.0–10.2],  $P = 0.812$ ).

### Features of Serial Bone Biopsies

In 3 cases, biopsies of the posterior-superior iliac crest were taken at more than 1 time point, before and during treatment with different anticancer therapies. Two of these cases were initially biopsied in the presence of disease responding to therapy based on the PCWG2 criteria; in these posttreatment biopsies, median ADCs were high with biopsy analyses identifying no tumor cells. At disease progression established according to PCWG 2 criteria, however, median ADCs decreased and repeated bone biopsies detected tumor cells (Fig. 2).

**TABLE 4.** Univariate and Multivariate Logistic Regression Models With Bone Marrow Positivity as the Dependent Variable

	OR	95% CI	<i>P</i>
Univariate logistic regression model			
MRI Parameters			
Median ADC	0.99	0.99–1.00	0.002
Median nDWI signal intensity	1.57	1.01–2.43	0.045
Signal-weighted fat fraction	0.96	0.94–0.99	0.008
Histological parameters			
Osteoid score	3.14	1.19–8.31	0.021
Fibrosis score	4.02	1.68–9.61	0.002
Trabecular volume	1.02	0.98–1.06	0.276
Fat content	0.92	0.88–0.97	0.001
Multivariate logistic regression model			
Median ADC	0.99	0.97–1.00	0.050
Osteoid score	6.34	0.04–1040.72	0.478
Fibrosis score	15.40	0.32–748.75	0.168

ADC indicates apparent diffusion coefficient; CI, confidence interval; MRI, magnetic resonance imaging; nDWI, normalized b900 diffusion-weighted imaging; OR, odds ratio.

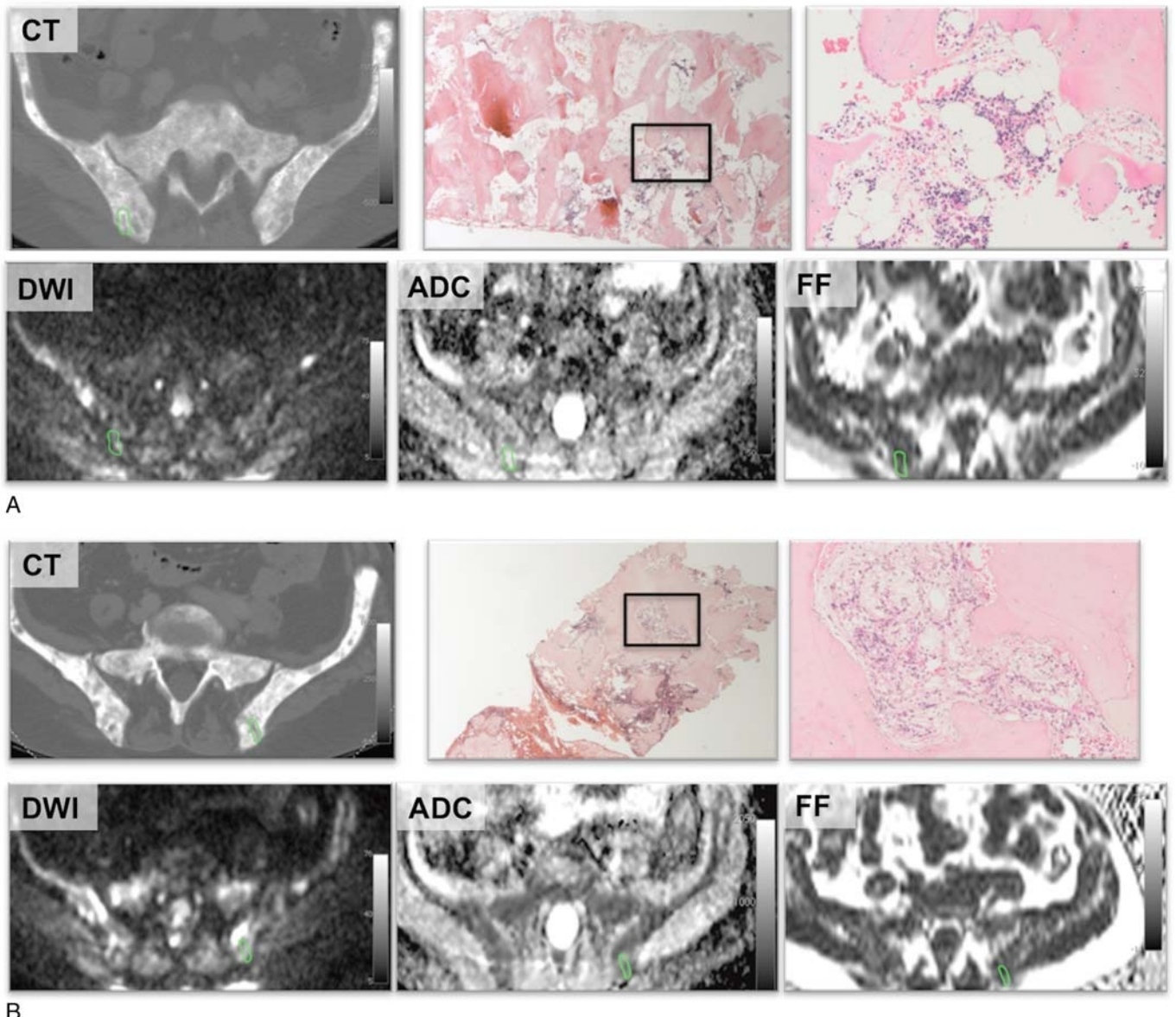


**FIGURE 2.** A 79-year-old man with widespread bone metastases, CT, MP-MRI (DWI, ADC, and FF), and bone biopsy histology during disease response (A) and at disease progression (B) to abiraterone. A green ROI delineating the biopsy tract on CT imaging was transferred to registered MRI sequences (DWI b900, ADC map, and FF map). The bone biopsies were decalcified, processed, and stained with hematoxylin and eosin. A black rectangle in  $\times 40$  panel marks the region depicted in the  $\times 200$  panel. Median nDWI signal intensity in the area of the bone biopsy during disease response (A) was lower than at disease progression (B) ( $2$  vs  $5$ ), whereas median ADC values and swFF were higher during disease response (A) than at disease progression (B) ( $1342 \times 10^{-6} \text{ mm}^2/\text{s}$  vs  $899 \times 10^{-6} \text{ mm}^2/\text{s}$ ;  $20\%$  vs  $13\%$ , respectively). In concordance with MRI parameters, despite both biopsies being targeted to imaged bone metastases, the bone biopsy at disease response (A) was negative for tumor cells and had  $30\%$  fat content, whereas at disease progression (B), the bone biopsy was positive for tumor cells and had  $5\%$  fat content.

In the third patient with serial bone biopsies, a 74-year-old man with mCRPC who had received previous radiotherapy to the pelvis before the first biopsy, the median ADC of the biopsied iliac crest was similar at the 2 time points ( $1668 \times 10^{-6} \text{ mm}^2/\text{s}$  and  $1968 \times 10^{-6} \text{ mm}^2/\text{s}$ , respectively), with both biopsies being negative for tumor cells. These high ADC values would be consistent with maintained response to previous radiotherapy.

## DISCUSSION

In this study, we correlated MP-MRI parameters of bone metastases, and of nonmalignant bone, with bone marrow biopsy histological

and molecular features in treated patients with CRPC. These findings contribute to the clinical qualification of MP-MRI as a biomarker of mCRPC. We have shown that MP-MRI features including nDWI signal intensity, ADC values, and swFF successfully differentiate non-metastatic bone from bone metastases in CRPC patients. The nDWI signal intensity and ADC values in normal bone marrow in our population were similar with those previously described<sup>18</sup>; these are closer to the described values in yellow bone marrow than in red bone marrow, in line with the high swFF observed in our study. These are consistent with the advanced age of our population and chronic exposure to hormonal ablation for prostate cancer treatment. Low signal intensity and

low ADC values of yellow bone marrow are likely to be related to an abundance of fat cells and reduced water proton density.

Within the bone metastases cohort, MP-MRI parameters predicted the presence and degree of cellularity of metastatic disease in bone biopsies. In this heavily pretreated population, the absence of tumor in negative biopsies likely reflects tumor cell kill after prior treatments. We have shown a significant inverse correlation of ADC and swFF, and a significant positive correlation of nDWI signal intensity with bone metastasis tumor cellularity burden. This supports using MP-MRI to guide bone biopsy acquisition in mCRPC for molecular and histological studies. Our studies do indicate, however, that ADC values and nDWI signal are also influenced by other histological findings, such as the presence of osteoid and fibrosis in biopsies. Nevertheless, when controlling for fibrosis and osteoid in multivariate analysis, median ADC was still independently correlated with tumor cellularity. Furthermore, by using DWI b50 rather than b0 as our low *b*-value in the DWI acquisition, we have reduced the influence of blood flow variability on calculated ADC values. Lastly, in our study, MRI parameters including ADC, nDWI and swFF were more informative of active versus nonactive bone metastases when compared with CT scan bone HU.

We acknowledge potential limitations of our study; first, our pilot sample size is small, although still representing the largest series presented to date of bone biopsy to MP-MRI correlative studies for this disease. Furthermore, external validity of the performance of these biomarkers by receiver operating characteristic curve and linear discriminant analysis is limited, due to the absence of a validation cohort. Analyzing larger populations in prospective, multicenter validation studies is now warranted for validation of these results. Second, the retrospective nature of this study may have led to some bias; patients have been previously treated with different drugs including 10 patients who received bisphosphonates; this may account for differences in the MRI parameters, although, the number of patients was small for performing subgroup analyses. Ideally, the MRI, CT, BS, and bone biopsy should have been obtained simultaneously. However, we consider that the 12-week maximum interval between the scans and biopsy is reasonable considering the retrospective nature of this study and should not have substantially impacted these results. Moreover, MRI, CT, and BS assessments were always performed before the bone biopsy, avoiding artifacts secondary to the biopsy procedure. Third, we estimated the bone marrow fat as the swFF based on a 2-echo Dixon sequence instead of multiecho acquisition, which would allow a more reliable proton density FF quantification.<sup>23,30</sup> Fourth, histopathological analyses were performed with core-needle biopsies and the small area of the drawn ROIs on MRI and CT may not have been representative of tumor heterogeneity. Finally, further studies correlating MRI with histopathology features from CT-guided bone metastases in areas outside the pelvis, more prone to MRI artifacts, maybe of interest to validate these results in bone metastases throughout the skeleton.

Overall, MP-MRI is a powerful noninvasive biomarker of the histological features of bone metastases in prostate cancer. Multiparametric MRI differentiates normal bone marrow from bone metastases, and also bone metastases with detectable tumor cells from those without tumor cells at biopsy, which can aid bone biopsy guidance. Finally, we have reported that changes in DWI parameters and histological features parallel tumor progression and regression, probably as a result of response to treatment. Overall, these findings, together with recent published clinical studies,<sup>31,32</sup> further support the clinical utility of MP-MRI as a biomarker of bone metastases in mCRPC.

#### ACKNOWLEDGMENTS

The authors thank David Lorente, Mihaela Rata, Matthew D. Blackledge, Susana Miranda, Mateus Crespo, Ana Ferreira, Ruth Riisnaes, Zafeiris Zafeiriou, Mariane Sousa, Pasquale Rescigno, Diletta

Bianchini, David J. Collins, and Martin O. Leach for their contribution to this manuscript.

This study was supported by Prostate Cancer UK (PG14-016-TR2), Prostate Cancer Foundation (20131017), Stand Up To Cancer (SU2C-AACR-DT0712), Movember Foundation (Movember-Prostate Cancer UK Centre Grant CEO13-2-002), and Cancer Research UK (C347/A18077 and CRUK C1060/A16464). J.M. was supported by an Art Kern-Prostate Cancer Foundation Young Investigator Award and an MRC-Prostate Cancer UK-Movember Fellowship. Support was also provided by an Experimental Cancer Medicine Centre Grant and the National Institute for Health Biomedical Research Centre to the Royal Marsden. R.P.L. conducted this work in the Medicine Doctorate framework of the Universitat Autònoma de Barcelona.

#### REFERENCES

- de Bono JS, Logothetis CJ, Molina A, et al. Abiraterone and increased survival in metastatic prostate cancer. *N Engl J Med*. 2011;364:1995–2005.
- Scher HI, Fizazi K, Saad F, et al. Increased survival with enzalutamide in prostate cancer after chemotherapy. *N Engl J Med*. 2012;367:1187–1197.
- Parker C, Nilsson S, Heinrich D, et al. Alpha emitter radium-223 and survival in metastatic prostate cancer. *N Engl J Med*. 2013;369:213–223.
- de Bono JS, Oudard S, Ozguroglu M, et al. Prednisone plus cabazitaxel or mitoxantrone for metastatic castration-resistant prostate cancer progressing after docetaxel treatment: a randomised open-label trial. *Lancet*. 2010;376:1147–1154.
- Halabi S, Kelly WK, Ma H, et al. Meta-analysis evaluating the impact of site of metastasis on overall survival in men with castration-resistant prostate cancer. *J Clin Oncol*. 2016;34:1652–1659.
- Robinson D, Van Allen EM, Wu YM, et al. Integrative clinical genomics of advanced prostate cancer. *Cell*. 2015;161:1215–1228.
- Lorente D, Omlin A, Zafeiriou Z, et al. Castration-resistant prostate cancer tissue acquisition from bone metastases for molecular analyses. *Clin Genitourin Cancer*. 2016;14:485–493.
- Eisenhauer EA, Therasse P, Bogaerts J, et al. New response evaluation criteria in solid tumours: revised RECIST guideline (version 1.1). *Eur J Cancer*. 2009;45:228–247.
- Scher HI, Morris MJ, Stadler WM, et al. Trial design and objectives for castration-resistant prostate cancer: updated recommendations from the prostate cancer clinical trials working group 3. *J Clin Oncol*. 2016;34:1402–1418.
- Liu LP, Cui LB, Zhang XX, et al. Diagnostic performance of diffusion-weighted magnetic resonance imaging in bone malignancy: evidence from a meta-analysis. *Medicine (Baltimore)*. 2015;94:e1998.
- Guo AC, Cummings TJ, Dash RC, et al. Lymphomas and high-grade astrocytomas: comparison of water diffusibility and histologic characteristics. *Radiology*. 2002;224:177–183.
- Hayashida Y, Hirai T, Morishita S, et al. Diffusion-weighted imaging of metastatic brain tumors: comparison with histologic type and tumor cellularity. *AJNR Am J Neuroradiol*. 2006;27:1419–1425.
- Zelhof B, Pickles M, Liney G, et al. Correlation of diffusion-weighted magnetic resonance data with cellularity in prostate cancer. *BJU Int*. 2009;103:883–888.
- Liu Y, Ye Z, Sun H, et al. Clinical application of diffusion-weighted magnetic resonance imaging in uterine cervical cancer. *Int J Gynecol Cancer*. 2015;25:1073–1078.
- Matsubayashi RN, Fujii T, Yasumori K, et al. Apparent diffusion coefficient in invasive ductal breast carcinoma: correlation with detailed histologic features and the enhancement ratio on dynamic contrast-enhanced MR images. *J Oncol*. 2010;2010.
- Park SH, Choi HY, Hahn SY. Correlations between apparent diffusion coefficient values of invasive ductal carcinoma and pathologic factors on diffusion-weighted MRI at 3.0 Tesla. *J Magn Reson Imaging*. 2015;41:175–182.
- Chen L, Liu M, Bao J, et al. The correlation between apparent diffusion coefficient and tumor cellularity in patients: a meta-analysis. *PLoS One*. 2013;8:e79008.
- Padhani AR, van Ree K, Collins DJ, et al. Assessing the relation between bone marrow signal intensity and apparent diffusion coefficient in diffusion-weighted MRI. *AJR Am J Roentgenol*. 2013;200:163–170.
- Messiou C, Collins DJ, Morgan VA, et al. Optimising diffusion weighted MRI for imaging metastatic and myeloma bone disease and assessing reproducibility. *Eur Radiol*. 2011;21:1713–1718.
- Dietrich O, Geith T, Reiser MF, et al. Diffusion imaging of the vertebral bone marrow. *NMR Biomed*. 2015.
- Hillengass J, Bauerle T, Bartl R, et al. Diffusion-weighted imaging for non-invasive and quantitative monitoring of bone marrow infiltration in patients with monoclonal plasma cell disease: a comparative study with histology. *Br J Haematol*. 2011;153:721–728.

22. Nonomura Y, Yasumoto M, Yoshimura R, et al. Relationship between bone marrow cellularity and apparent diffusion coefficient. *J Magn Reson Imaging*. 2001;13:757–760.
23. Le Ster C, Gambarota G, Lasbleiz J, et al. Breath-hold MR measurements of fat fraction, T1, and T2 \* of water and fat in vertebral bone marrow. *J Magn Reson Imaging*. 2016;44:549–555.
24. Daldrup-Link HE, Henning T, Link TM. MR imaging of therapy-induced changes of bone marrow. *Eur Radiol*. 2007;17:743–761.
25. Teman CJ, Wilson AR, Perkins SL, et al. Quantification of fibrosis and osteosclerosis in myeloproliferative neoplasms: a computer-assisted image study. *Leuk Res*. 2010;34:871–876.
26. Ferraldeschi R, Nava Rodrigues D, Riisnaes R, et al. *PTEN* protein loss and clinical outcome from castration-resistant prostate cancer treated with abiraterone acetate. *Eur Urol*. 2015;67:795–802.
27. Rosset A, Spadola L, Ratib O. OsiriX: an open-source software for navigating in multidimensional DICOM images. *J Digit Imaging*. 2004;17:205–216.
28. Insight Segmentation and Registration Toolkit (ITK). Available at: <http://itk.org>. Accessed February 6, 2017.
29. Ulmert D, Kaboteh R, Fox JJ, et al. A novel automated platform for quantifying the extent of skeletal tumour involvement in prostate cancer patients using the bone scan index. *Eur Urol*. 2012;62:78–84.
30. Karampinos DC, Melkus G, Baum T, et al. Bone marrow fat quantification in the presence of trabecular bone: initial comparison between water-fat imaging and single-voxel MRS. *Magn Reson Med*. 2014;71:1158–1165.
31. Blackledge MD, Collins DJ, Tunari N, et al. Assessment of treatment response by total tumor volume and global apparent diffusion coefficient using diffusion-weighted MRI in patients with metastatic bone disease: a feasibility study. *PLoS One*. 2014;9:e91779.
32. Perez-Lopez R, Mateo J, Mossop H, et al. Diffusion-weighted imaging as a treatment response biomarker for evaluating bone metastases in prostate cancer: a pilot study. *Radiology*. 2017;283:168–177.